Technical Report No. 32-648

The Effects of Injection Mass Flux Distributions And Resonant Combustion on Local Heat Transfer in a Liquid-Propellant Rocket Engine

Jack H. Rupe

George I. Jaivin

ipl

JET PROPULSION LABORATORY
CALIFORNIA INSTITUTE OF TECHNOLOGY
PASADENA, CALIFORNIA

October 1, 1964
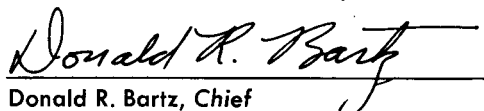
Technical Report No. 32-648

The Effects of Injection Mass Flux Distributions And Resonant Combustion on Local Heat Transfer in a Liquid-Propellant Rocket Engine

Jack H. Rupe

George I. Jaivin

Donald R. Bartz, Chief
Propulsion Research Section

CONTENTS

TABLE

FIGURES

FIGURES (Cont'd)

ABSTRACT

13277

Local values of the heat transfer rates in a particular liquid-propellant rocket engine–injector configuration are presented. It is shown that during stable, relatively quiescent combustion, the local heat transfer rates in the chamber vary axially over a range of 0.5 to 4.0 Btu/in² sec, and circumferentially, at a station somewhat upstream from the nozzle entrance, over a range from 0.5 to 6.0 Btu/in² sec. Both heat transfer gradients can be as high as 5.0 Btu/in² sec/in., and the distribution is extremely sensitive to small changes in injection properties, i.e., gross mixture ratio, with the consequent changes in mass and mixture ratio distribution near the wall.

Initial attempts to correlate these data with the injection scheme, as characterized by the properties of non-reactive sprays, have indicated that the boundary flow, and therefore the heat transfer rate, is dominated by the proximity of the propellant to the wall. It is therefore suggested that a quantitative correlation between these properties and local heat transfer rates in the chamber is possible and could ultimately lead to the *a priori* specification of a controlled, compatible boundary flow. To this end, some preliminary efforts to illustrate the significance of "the propellant mass flux arriving at the wall" are presented.

The local heat flux distribution attained during resonant combustion is also presented and is compared with values for stable combustion.

author

INTRODUCTION*

The heat transfer aspects of a liquid-propellant rocket engine have historically been described in terms of

---

*The information contained in this Report was presented at the Sixth Liquid-Propulsion Symposium of the Chemical Propulsion Information Agency (CPIA), held in Los Angeles, California, on Sept. 23–25, 1964, and was published in the *Bulletin of the Sixth Liquid Propulsion Symposium* (CPIA Publication 56, August 1964) under the title "Experimental Measurements of Local Heat Transfer in a Liquid-Propellant Rocket Engine."

the gross characteristics of the propellant system, i.e., the equilibrium temperature of the reaction products, the thermodynamic properties of those gases, the flow-area-averaged mass flux, the local Mach number, and a particular geometrical configuration. This is relatively successful with respect to flow in a nozzle where a model that assumes chemical equilibrium and uniform one-dimensional flow has been experimentally supported by a number of investigations (Refs. 1–4).

However, within the confines of the chamber itself (and to a lesser extent along the boundary in the vicinity of the nozzle throat), it is well known that such correlations tend to break down. As noted in Ref. 5, Bartz summarized the situation by saying ". . . the reliable prediction of heat flux in a combustion chamber is not possible because of the inadequate status of quantitative knowledge of rocket-engine combustion phenomena" and pointed out that each injector has " . . . its own peculiar flow and energy release pattern" and that ". . . these peculiarities . . . directly influence the heat-flux distribution." The peculiarities that he mentions must certainly include variations in local mixture ratio and mass flux (and hence, temperature and velocity) which are produced near the injection plane and tend to persist down the chamber wall, through the throat and out the nozzle exit.

This situation can be additionally complicated by direct impingement of liquid propellant on the chamber boundary, either intentionally for purposes of producing a cool boundary flow, or inadvertently, as a consequence of an injection scheme that attempts to utilize the volume near the wall for combustion purposes. This liquid impingement produces a boundary flow that undergoes a transition from a complex two-phase flow near the wall, which is probably associated with a liquid film on the wall, to a gas boundary layer of varying composition as the liquid evaporates and/or reacts on the surface and moves downstream to the throat. Thus, it is extremely unlikely that the relatively simple convective heat transfer equations based on flow-area-averaged one-dimensional parameters will be suitable to characterize this situation, and a much more realistic model must be generated before reasonable *a priori* estimates of combustion chamber heat transfer rates can be formulated.

Experimental measurements of heat transfer to combustion chamber walls have, for the most part, been restricted to the calorimetric methods that are typified by the work of Welsh and Witte (Ref. 6) and Witte and Harper (Ref. 7). In this case, the heat transfer at any axial station was averaged over the complete circumference for an incremental length and, therefore, is insensitive to any circumferential variations.

It is true, of course, that such measurements are adequate for determining total heat load (and the "averaged" axial distribution of load) but it should be recognized that, if large circumferential variations do exist, it may be possible to exceed the allowable local heat transfer rates and, hence, produce local failure. Such failures become increasingly important as engine designs become more sophisticated and are pushed to higher over-all performances, and particularly in the determination of the compatibility of ablative materials and radiatively cooled chambers. In these latter cases the necessity for providing an extra margin to cover local variations can produce substantial weight penalties, or even preclude the use of an otherwise more desirable material.

It is, therefore, important that the presence of these variations be predictable from, and if possible, correlatable in a quantitative sense with, the injection scheme and its geometrical relationship to the combustion chamber wall. It is to this end that the information presented herein was assembled and, although the correlation is far from complete, it seems clear that the properties of the boundary flow are, in fact, uniquely related to the injection scheme and, therefore, should be correlatable with the significant injection parameters. This last statement presumes, of course, that the injection scheme will provide a steady, stable, reproducible environment at the wall.

The distributions of local heat transfer to a combustion chamber wall that are presented here were obtained as part of a performance evaluation of a series of injection schemes that were intended to demonstrate the applicability of the mass and mixture ratio data obtained with non-reactive fluids to the design of actual reacting systems. The injectors emphasized stable, reproducible, controlled hydraulics and an injector element orientation that was intended to maximize the uniformity of the distribution of the axial mass flux. The former criteria resulted in stable, reproducible boundary flows and the latter produced marked nonuniformities on the chamber circumference and, hence, an opportunity to attempt a gross correlation between injection properties and local heat flux to the wall. Typical results for steady-state combustion are presented, and the influence of changes in detailed operating characteristics of the injector is illustrated. It is intended that these results should be a statement of the physical nature of the problem as highlighted by the observations made thus far, and it is hoped that they will serve to indicate the direction that must be taken by more sophisticated experiments and analysis that will lead to a generally valid correlation or theory.

II. EXPERIMENTAL APPARATUS AND TECHNIQUES

A. Engine Characteristics

An uncooled, heavy-wall construction, liquid-propellant rocket engine producing 20,000 lb of thrust at sea level was used in this experimental program. An assembly drawing of the complete engine configuration, which is geometrically similar to the so-called "Corporal engine," and hence is designated the "uncooled Corporal engine," is shown in Fig. 1. The steel combustion chamber was 0.75 in. thick and had an inside diameter of 11.046 in. The nozzle was fabricated from copper and had a throat diameter of 7.756 in. The corresponding engine contraction ratio was 2.028. A steel nozzle extension having a 0.25-in.-thick wall was used to provide a nozzle expansion ratio of 4.578. At the nominal chamber pressure of 300 psia, this expansion ratio caused the nozzle flow to be somewhat overexpanded at the exit
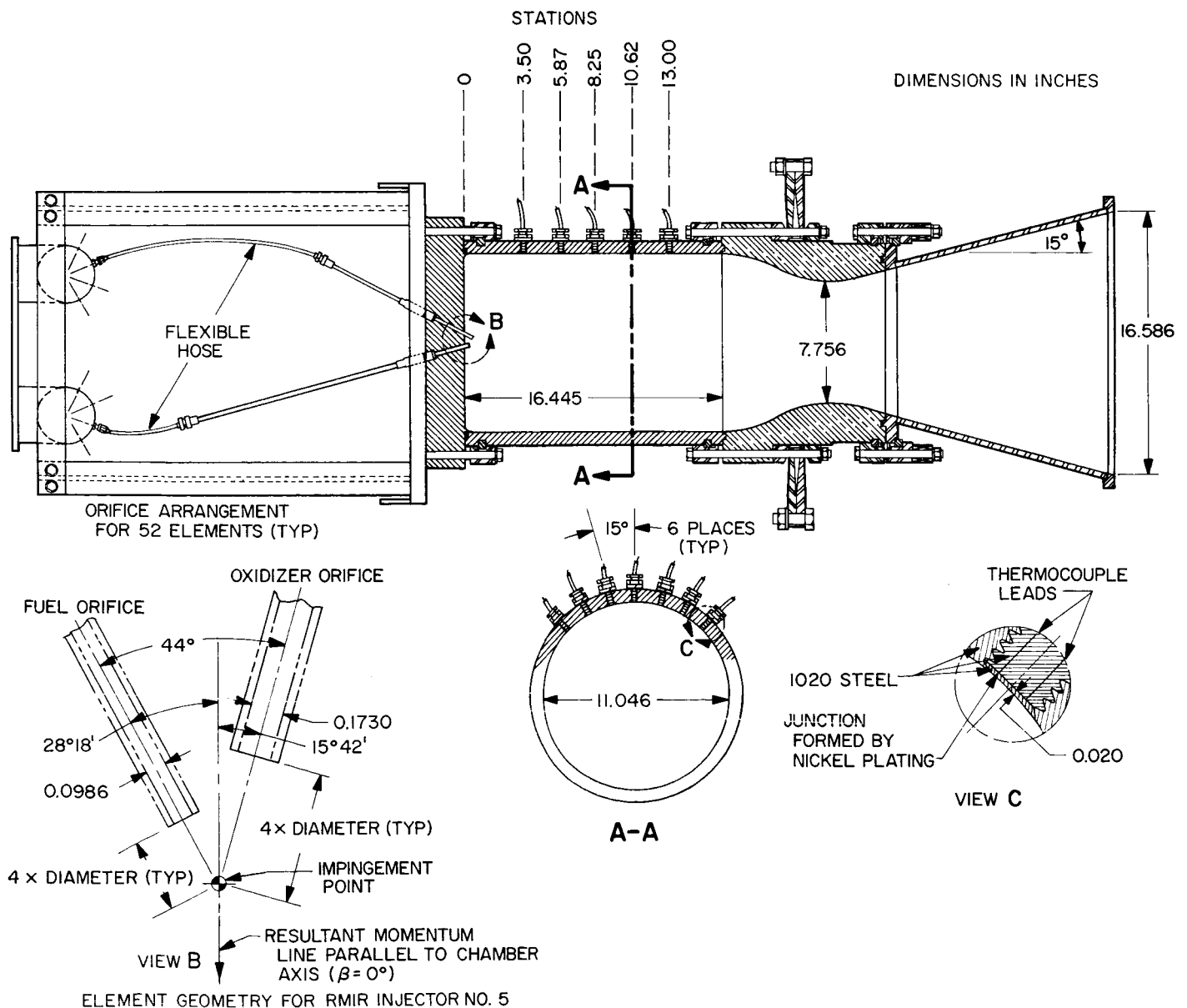

Fig. 1. Sketch of 20,000-lb-thrust engine and components used for chamber heat transfer measurements

plane, i.e., to approximately 9.7 psia, whereas the nominal ambient pressure at the Edwards Test Station (ETS) is 13.5 psia. The propellants used were SFNA[1] and Corporal fuel.[2] The peak performance for this propellant system is achieved at a mixture ratio ($\dot{w}_{ox}/\dot{w}_{fuel}$) of 2.80, but the engine was successfully operated over a mixture ratio range from 1.93 to 3.19. The characteristic chamber length L^*, was 40 in. A photograph of the complete engine assembly mounted in the test stand is shown in Fig. 2.

Although, as indicated above, this engine was, in most respects, geometrically similar to the uncooled Corporal

---

[1] SFNA (stabilized fuming nitric acid) consists of a mixture of the following compounds with percentages by weight as noted: 81.3–84.5% HNO_3; 14.0 ±1.0% NO_2; 2.5 ±0.5% H_2O; 0.6 ±0.1% HF.

[2] Corporal fuel consists of a mixture of the following compounds with percentage by weight as noted: 46.5 ±0.2% furfuryl alcohol ($C_4H_3OCH_2OH$); 7.0 ±0.2% N_2H_4; 1.5% max. H_2O; 0.7% max. impurities; remainder, aniline ($C_6H_5NH_2$).

configuration, it incorporated an injector design that had been utilized to demonstrate the relative significance of the non-reactive properties of the injection scheme to the combustion process as inferred from the over-all performance of the rocket engine system. The optimization of the injection system was predicated upon the simultaneous accomplishment of two objectives: (1) the achievement of a uniform distribution of the injected propellants within the combustion chamber; and (2) the effective mixing of the propellants in a manner that would cause the local mixture ratio throughout the chamber to be equal to the nominal mixture ratio. Ideally, moreover, such mass and mixture ratio distributions must be produced in a controlled and reproducible fashion.

In an attempt to build an injection system that satisfied these objectives, emphasis was placed upon the utilization of data acquired from hydraulic evaluations of sprays of non-reactive liquids. Earlier work with such fluids (Ref. 8) had shown that a near-uniform

ENGINE CONSTANTS

A_t = 47.15 in.^{2}

ϵ_e = 4.578

ϵ_c = 2.030

$(C_f)_{expected}$ = 1.410 λ C_d = 1.362

ASSUMING

γ = 1.25

P_c = 300 psia

P_0 = 13.5 psia

λ = 0.984 (15°)

C_d = 0.985

F = 19,300 lb

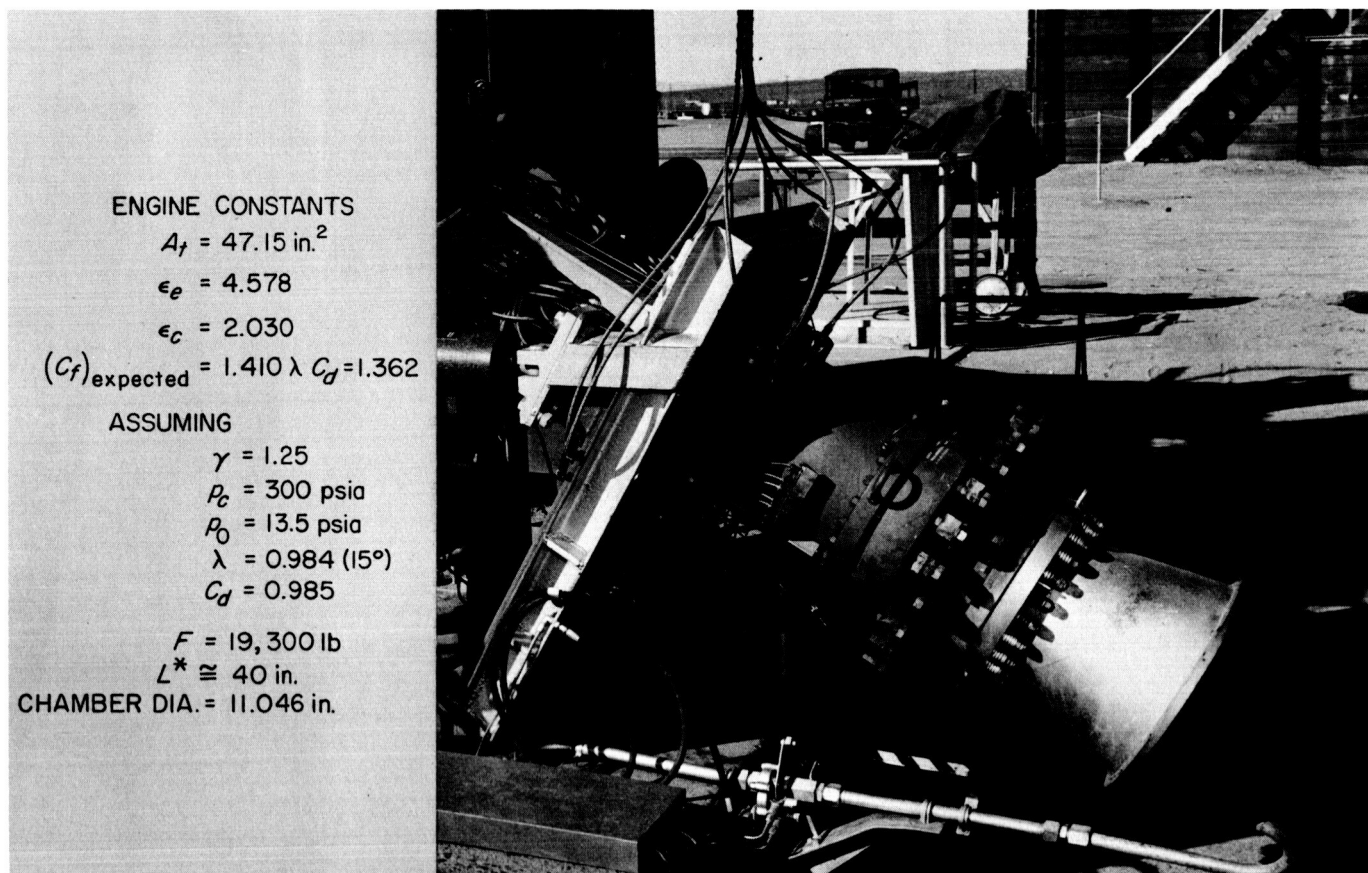$L^* \cong$ 40 in.

CHAMBER DIA. = 11.046 in.

Fig. 2. Typical test stand installation (ETS "B" Stand) for uncooled Corporal engine

mixture ratio can be achieved throughout a spray formed by two unlike impinging liquid streams when the product of the velocity-head ratio and the diameter ratio for the two streams is unity. Thus, a typical doublet element, which simultaneously satisfies the mixture-ratio-uniformity criterion stated above for the specific design mixture ratio and the propellant combination, has an orifice diameter ratio (oxidizer/fuel) of 1.755. A 44-deg impingement angle was used in order to retain geometrical similarity with the so-called Corporal injector element. The fluid velocities were 138 ft/sec and 87 ft/sec respectively for the fuel and oxidizer jets.

In order to provide the required controlled and reproducible hydrodynamic properties of the impinging jets, and hence assure similar characteristics in the sprays, the injector incorporated orifices of 100 diameters length which produced fully developed turbulent velocity profile jets at the orifice exit. Thus, these criteria, as set forth in Ref. 9, were satisfied. Further, this technique grossly attenuated flow disturbances associated with possible maldistributions occurring within the supply manifold.

The mass distribution of the spray from a typical element was determined by sampling a spray formed with non-reactive liquids that simulated the actual propellants. This sampling was accomplished by positioning an array of collection tubes in the spray in a manner that caused the local samples to be obtained at points equidistant from the point of intersection of the center-lines of the two streams, i.e., the impingement point. The non-reactive fluids that were used were immiscible and, hence, the relative volumes of the two liquids collected in a given tube were indicative of the local mixture ratio, while the total sample volume represented the local mass flux. Additional details of the sampling procedure can be found in Ref. 10.

The mass distribution analogue obtained in this manner from a typical injector element that was operated at a mixture ratio of 2.80 is shown in Fig. 3. The pattern represents the axial mass distribution that would be observed on a flat plane perpendicular to the resultant momentum line of the spray. The contours, which serve to demarcate the several areas shown in the Figure, represent lines of constant mass flux per unit area and have the values noted. The area contained within each of the closed curves denotes a region containing the indicated fraction of the cumulative total mass of the spray. In the original model, the shading of each of these regions was made proportional to the mass flux which it represents. It should be noted that the outer boundary of the
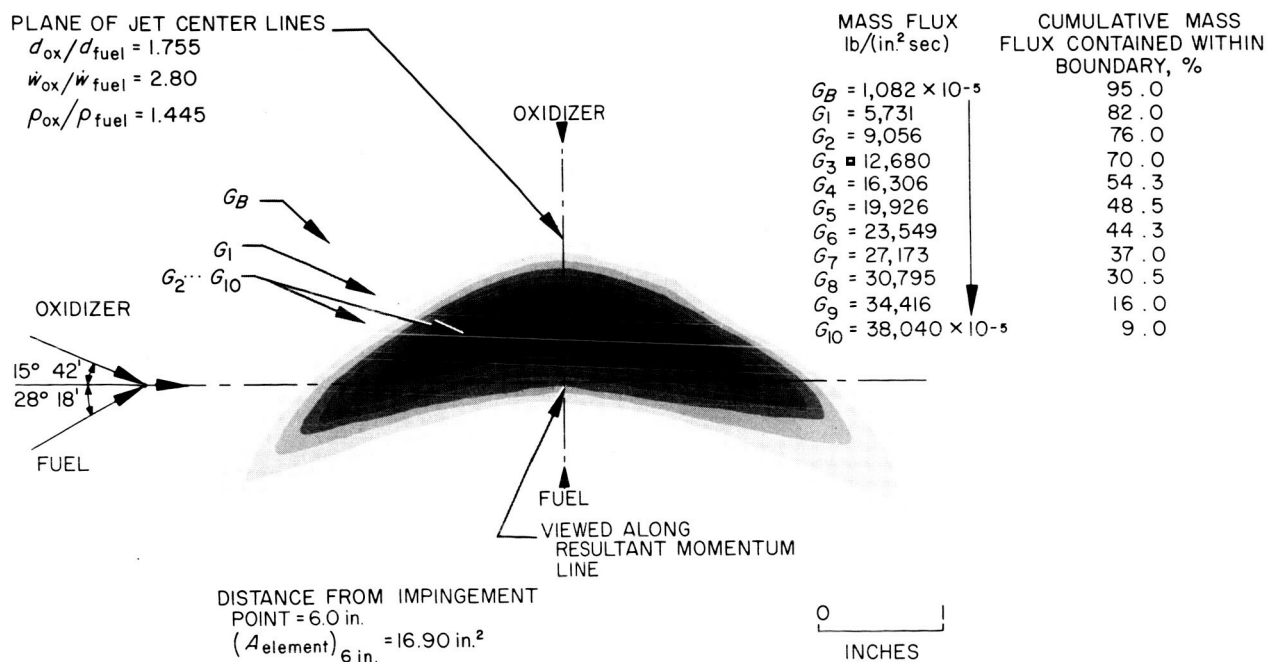

Fig. 3. Analogue of mass flux distribution of doublet element for RMIR Injector No. 5

pattern encircles 95% of the total sampled mass of the spray.

If it is assumed that the spray originates at the impingement point and that fluid particle trajectories are straight lines emanating from the spray source, then it follows that the size of the mass distribution pattern as shown in Fig. 3 is linearly related to the distance from the impingement point to the plane on which the mass distribution is displayed. Further, in order to establish a uniform distribution of mass throughout the combustion chamber, each injector element is expected to contribute a proportionate fraction of the total injected mass of the propellants to its share of the chamber cross-section. Accordingly, once the number of elements is specified, a distance can be determined such that the area enclosed within the outer boundary of the mass distribution pattern at that distance represents $1/N$ of the total cross-sectional area of the combustion chamber, where N is the total number of elements comprising the injector.

In this particular instance, N was specified to be identical with the number of elements contained in the Corporal injector, so that the area of each element corresponds to 1/52 of the chamber area. The distance that satisfied this requirement was designated the "model plane distance" and the corresponding plane was denoted as the "model plane." For this particular injector design, the model plane distance was 1.98 in., and the model plane was located 2.75 in. from the injector face since the impingement point plane is 0.77 in. from the injector face. Once this element configuration was specified, it then remained to arrange the 52 mass-distribution patterns on the model plane in a manner that effectively covered the chamber area without leaving obvious voids or mass concentrations. This was a trial-and-error procedure that finally resulted in the arrangement shown in Fig. 4. This particular injection configuration was but one of a series and was designated Rocket Motor Injection Research (RMIR) Injector No. 5.

The non-reactive properties of this particular injection scheme, together with those of six others, have been detailed in Ref. 11, and their performance evaluation has been presented in Ref. 12. This information will not be repeated here, but can be summarized by stating that the performance demonstrated by this engine is considered to be a valid and significant indication of the effectiveness of the application of non-reactive data to the logical design of a liquid propellant rocket engine. For example, it was shown that over the mixture ratio

range from 1.9 to 3.2, the percentages of the theoretical characteristic velocity c^* (based on equilibrium flow considerations) that were experimentally measured ranged from 98.8 to 98.0% (based on the stagnation pressure as determined from measurements made at the nozzle inlet) prior to any correction for heat transfer to the chamber and nozzle walls. Similarly, the percentage of the theoretical specific impulse I_s, experimentally measured (and uncorrected for changes in gamma or nonoptimum expansion effects), varied from 94.6 to 92.0% of the equilibrium values over this same mixture ratio range.

It should be noted that when this engine was initially tested, a serious combustion instability problem was encountered, but this problem was alleviated by mounting a set of baffles on the injector face. The arrangement of the baffles on the injector is illustrated in Fig. 4. With the baffles installed, the combustion processes were stable and the root-mean-square average pressure fluctuations that were measured were less than 1 psi. It was found, for identical operating conditions, that the performance data were reproducible within 0.5%, and that the presence of the baffles did not have any measurable effect on stable performance.

B. Heat Transfer Measurements

A transient thermocouple plug technique was used to determine the local heat flux in the uncooled rocket-engine chamber. The method is based on the solution of the radial, transient conduction equation for a homogeneous, hollow cylinder having known, but variable, thermal properties. The equation may be expressed as:

$$\rho c_p \frac{\partial T}{\partial t} = \frac{\partial}{\partial R}\left(k \frac{\partial T}{\partial R}\right) + \frac{k}{R} \frac{\partial T}{\partial R} \qquad (1)$$

With the specification of proper boundary conditions, the solution of this equation provides a complete temperature distribution through the chamber wall as a function of time. The boundary-condition information required is the time–temperature histories of two independent points that are on the same radial path in the engine wall, along with an initial temperature distribution between the points. The boundary information can be obtained from thermocouples placed on or within the chamber walls. An instantaneous value of the local heat flux at the inner chamber wall can be then computed by use of the Fourier-Biot equation as the product of the temperature gradient and the thermal conductivity at the inner surface.

RMIR INJECTOR NO. 5
FUEL—CORPORAL
OXIDIZER—SFNA
MIXTURE RATIO = 2.80

INJECTOR REFERENCE MARK
(VIEWED LOOKING UPSTREAM)

CHAMBER ANGLES
INCREASE CLOCKWISE

ELEMENT
NO. 9

BAFFLE
LOCATIONS

CHAMBER
BOUNDARY

IMPINGEMENT POINT PLANE AT STA. 0.767
MODEL PLANE AT STA. 2.747

$(G_{max})_{element}$ AT STA. 16.45 = 0.0627 lb/(in.^{2} sec)

0   I
INCHES
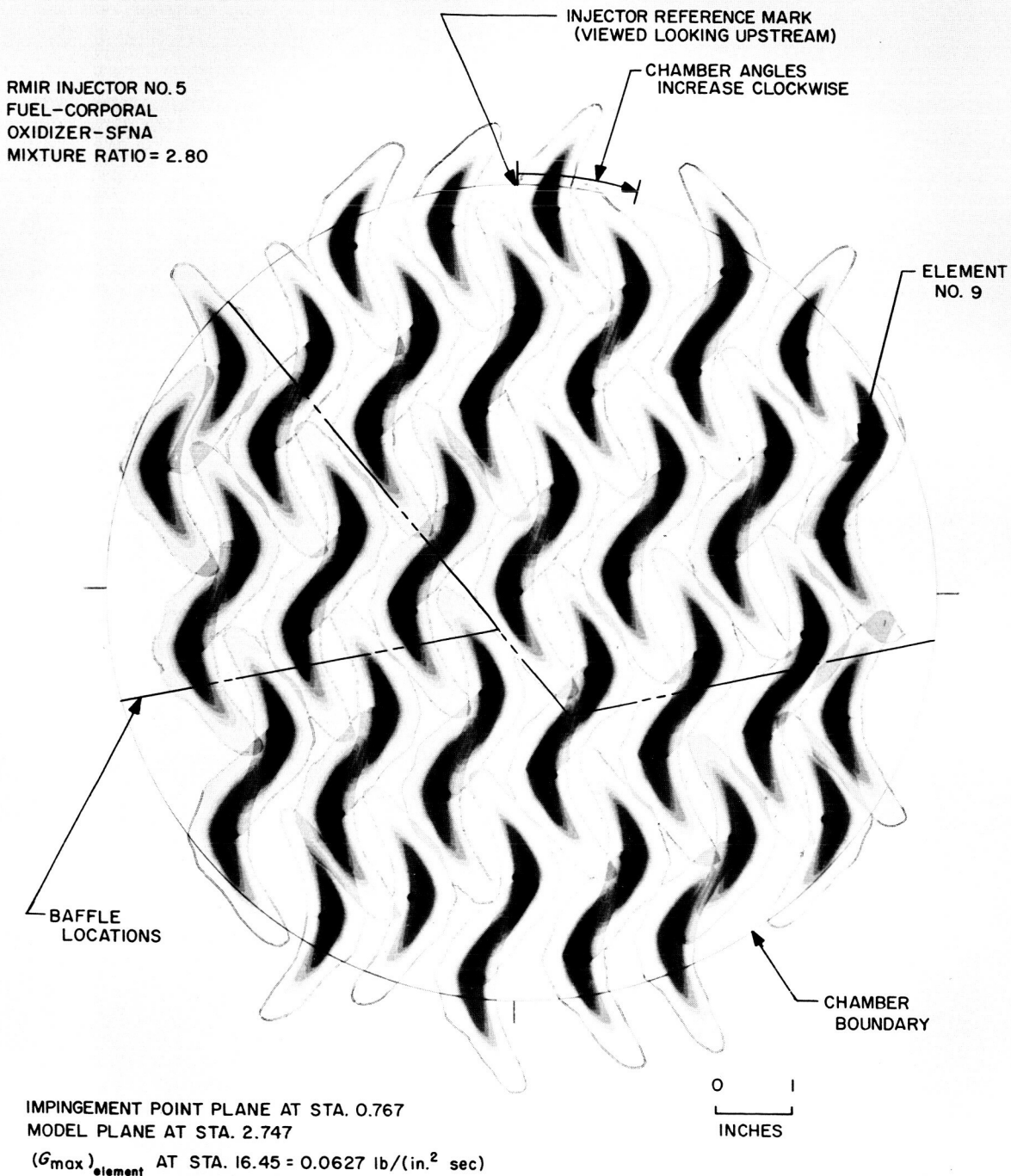
Fig. 4. Axial mass flux distribution model for RMIR Injector No. 5

The transient conduction equation (Eq. 1) that describes the change of temperature within the chamber wall with time and distance is a nonlinear, second-order, partial differential equation having no known analytical solution. However, a solution to this equation can be closely approximated by using standard numerical methods to transform the differential equation into a difference equation, which can then be solved on a digital computer. A derivation of the pertinent difference equation formulation as well as a detailed discussion of stability criteria and an evaluation of the accuracy of the numerical solution technique can be found in Ref. 13. A program

has been developed by the Jet Propulsion Laboratory Programming Analysis Group for the IBM 7094 computer and has been used to reduce the experimental data obtained in this investigation.

In order to minimize the errors associated with the determination of the temperature gradient at the inner surface, it is desirable to determine this temperature directly, and, as indicated in Ref. 13, this is sometimes done. However, in the experiments reported here, the innermost wall junctions were recessed 0.020 in. below the inner chamber surface because it was deemed essential to protect the thermocouple junctions from the corrosive environment of the reactants. The plugs used in these experiments were commercially available under the trade name Delta-Couple and are fabricated by Advanced Technology Laboratories, Mountain View, California. They are constructed of the same material

(1020 mild steel) as the chamber wall, in order to minimize any disturbances in the heat flux caused by variations in specific heat and conductivity. After the thermocouple plugs were positioned to locate the inner junction at the correct depth, they were locked in place by a lock nut and washer arrangement. The portion of the plug protruding into the chamber was cut off and the end was machined to conform to the inner contour of the wall. The second junction was welded to the outside of the chamber wall as nearly as possible on a radial line from the inner junction. Although the alignment of these two junctions was not exact, as the computational model required, the results were unaffected since the outer wall temperature was essentially constant during a typical run. This was a consequence of the thick chamber walls used (0.75 in.) and the normally short run durations (3 sec). A typical thermocouple plug installation is shown in Fig. 1.
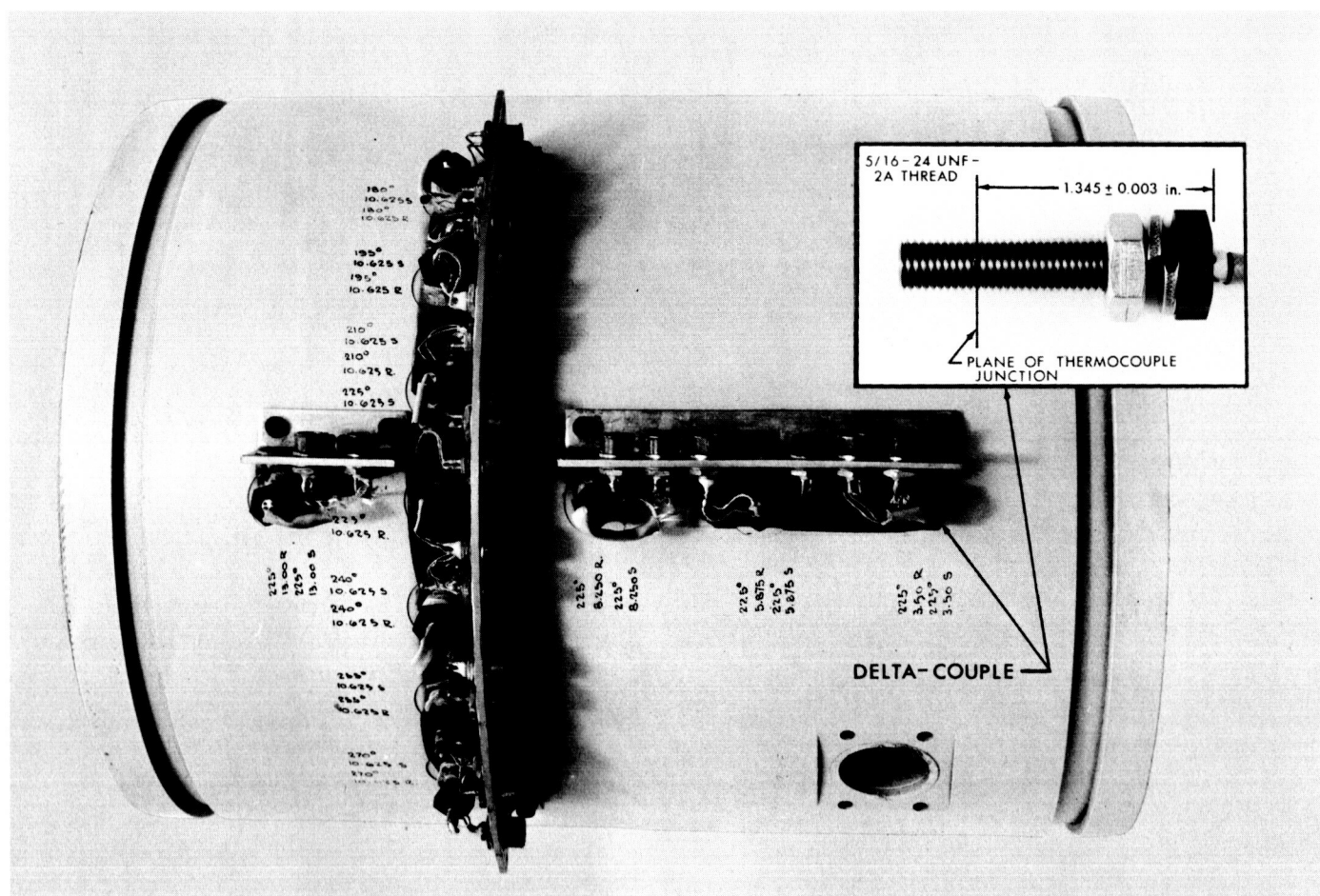

Fig. 5. Thermocouple installation in uncooled Corporal chamber

Eleven recessed and surface thermocouple pairs were mounted on the combustion chamber, and two pairs were installed in the injector face. Five of the thermocouple pairs on the chamber were positioned along a single axial line at stations corresponding to 3.50, 5.87, 8.25, 10.62 and 13.00 in. from the face of the injector (i.e., station 0). The other six were equally spaced 15 deg apart on the 10.62-in. axial station and were symmetrically located on each side of the axial row of thermocouples. In this manner a 90-deg quadrant of the circumferential temperature distribution could be surveyed simultaneously at the 10.62-in. axial station in increments of 15 deg, along with an axial temperature distribution along the length of the chamber. This arrangement is shown in Fig. 1, while Fig. 5 illustrates the appearance of the installed temperature instrumentation as well as the electrical termination and protective cover scheme used.

The outputs of the thermocouples were recorded on a CSC MicroSADIC[3] data acquisition system. Each thermocouple output was sampled approximately 55 times per second, converted to a digital format, and recorded on magnetic tape in a form immediately compatible with the input requirements of the digital computer heat transfer program. The computer was used (1) to calculate, as a function of time, the temperature distribution between the inner and outer thermocouple locations at each station, (2) to extrapolate the temperature distribution to the inner wall, and (3) to determine the inner wall temperature and local heat transfer flux rate.

The wall temperature–time histories that are evaluated in this scheme can be considered to be the experimental information, while the heat flux information is an analytical result that is directly derived from the former (i.e., through the Fourier-Biot equation). Thus the values of temperature and heat flux at any time are uniquely related to each other and, if it can be shown that there is a correspondence between the temperature distribution at a given time and the heat flux distribution at the same time, then either form of the information is sufficient for comparative purposes. In view of the fact that the wall temperature is much closer to the experimental

---

[3] Consolidated Systems Corporation Micro Sequential Analogue to Digital Incremental Converter.

measurement, in general, and is not susceptible to computer idiosyncrasies, it is preferred as a parameter to indicate the variations that exist in the chamber. Further attempts to normalize the heat flux data to reflect a common wall temperature, for example, cannot be justified in view of the uncertainties of the apparent film coefficients and/or the driving potentials.

In an effort to illustrate the correspondence of temperatures and heat flux, the paired values that were achieved after 2.0 sec of engine operation were plotted as shown in Fig. 6. It is clearly seen that there is, in fact, a one-to-one correspondence between the two quantities over the range encountered in the experiments, within a nominal variation of $\pm 10\%$ of the maximum recorded heat flux. Since this is more than adequate for illustrative purposes where both heat flux and temperature (at the designated time) varied by 400%, this close correspondence is used as justification for presenting the data as temperature distributions rather than heat flux. Obviously, the corresponding heat flux distributions can be produced with the help of Fig. 6, subject to the limitations noted above. It should be clearly recognized that this "correlation" applies only to this set of experimental measurements and is not intended to be generally applicable to other systems and/or transients.
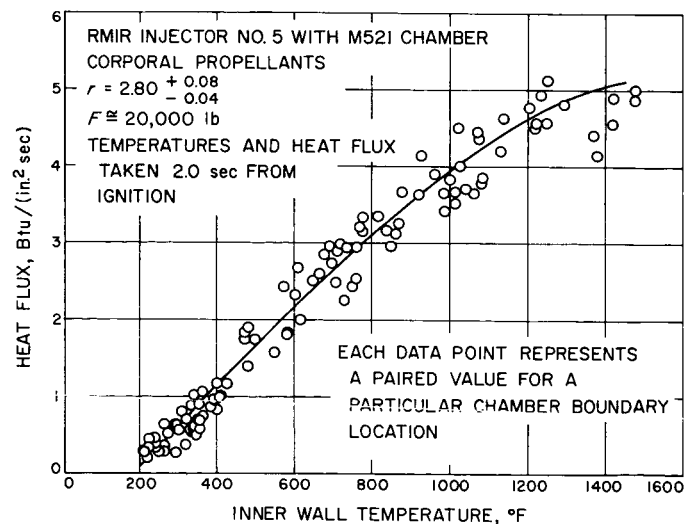

Fig. 6. Relating local, instantaneous, paired values of heat flux and temperature for the uncooled Corporal engine with RMIR Injector No. 5

III. EXPERIMENTAL TEMPERATURE DISTRIBUTIONS

A. Data Obtained at the Design Mixture Ratio

The inner-wall temperature-distributions that were measured in the combustion chamber of this particular engine configuration are shown in Fig. 7. A complete circumferential temperature distribution is displayed for the 10.62-in. axial station, along with several representative axial distributions. All data shown were measured 2.0 sec after the initiation of combustion within the chamber. At this time in the run, a sufficient amount of steady-state data had been supplied to the computer to be assured of a solution free from any effects induced by the starting transient. Since, as indicated in Section II-B, the circumferential array of thermocouples located at the 10.62-in. axial station was equally spaced in 15-deg increments and covered only a 90-deg quadrant of the chamber's periphery, it was necessary to make 12 separate engine tests in order to obtain the 5-deg resolution shown. Thus, it was essential that run conditions be held as nearly constant as possible. To this end the mixture ratio was maintained at a value of $2.80^{+0.05}_{-0.04}$. Also, it was found that simultaneous injection of both propellants into the chamber produced short, smooth start transients with virtually no over-pressure. The chamber pressure reached approximately 60% of its nominal value of 300 psia after 20–30 msec, and essentially steady-state conditions were achieved after 200–250 msec of operation. The reproducibility of the data is indicated in Fig. 7 where the end points of the quadrants overlapped, resulting in two temperature determinations being made at presumably the same location. The agreement is considered rather good, with the observed differences attributable to slight, inadvertent misalignments of the chamber relative to the injector as the chamber was rotated between the runs. As previously noted, at this design mixture ratio for the injector and engine, a combustion efficiency of 98% of the theoretical equilibrium flow c^*, with an rms pressure fluctuation of less than 1 psi, was maintained.

It is conventional when rocket engine performance data are presented to associate an "average" combustion chamber heat flux rate with a given set of other engine specifications. However, even a casual appraisal of the data given in Fig. 7 will suffice to illustrate the dangers inherent in such a procedure. It can be seen, for instance, that local temperatures differ by a factor of 5 in some instances, with similar variations to be expected in the heat flux rates. It is further noted that circumfer-

ential gradients exceed 1400°F/deg chamber angle, which corresponds to some 5.0 Btu/(in.^{2} sec)/in. of circumference. Thus, an estimate of average heat transfer conditions based on local measurements made in the chamber can lead to erroneous conclusions, unless uniformity is verified by a relatively complete sampling of local conditions. It is significant to observe that there is not a unique one-to-one correspondence between high combustion efficiency and high heat transfer rates. It is apparent from the evidence at hand that the two are not self-dependent, and that other modifying influences upon the heat transfer mechanisms must also be of importance.

The local variations existing in the chamber heat flux can reasonably be expected to be related to the factors that serve to describe local boundary wall flow conditions. Local flow phenomena, such as velocity and pressure gradients interlinked with their associated combustion effects, are but two such factors that could affect heat flux rates. Since a rocket engine combustion chamber does not closely model a so-called "well-stirred reactor," it is quite plausible that some of the observed heat flux variations are a consequence of nonhomogenous combustion phenomena. It is well known that film cooling is an effective mechanism for controlling heat transfer rates in combustion devices. Injector elements located at points on the injector face that are close to the chamber boundaries may supply large quantities of partially unreacted propellants to the chamber wall. It is conceivable that such local concentrations of mass at the boundary provide local film-cooled regions that are reflected in the temperature variations already noted. It is important to recognize that all of the factors mentioned above are extremely difficult, if not impossible, to measure in an actual engine.

It was found that the variations in heat flux were not confined to specific axial positions. Striations or streaks, i.e., variations in the coloration and the emitted light intensity, were observed in the exhaust plume of the engine. These appeared to be related to the hot and cold zones noted on the combustion chamber boundary. Occasionally, after a run, it was possible to observe discolorations on the walls. These discolored zones, which extended down the length of the combustion chamber and through the nozzle, could be correlated with the temperature measurements. This correlation indicated a rather strong and sustained interrelationship between boundary

(a)

CHAMBER ANGLES INCREASE CLOCKWISE
FROM INJECTOR REFERENCE LINE

RUNS NO. 708, 709, 710
RUNS NO. 727, 728, 729 (STA. 5.83)

STATION 10.62
STATION 5.83

BAFFLE ORIENTATION

CHAMBER BOUNDARY
1/2 SIZE

WALL TEMPERATURE, °F

RUNS NO. 705, 714, 715

RUNS NO. 702, 703, 704

RUNS NO. 711, 712, 713

VIEWED UPSTREAM TOWARD INJECTOR

(b)

WALL TEMPERATURE, °F

EXTRAPOLATED
POINT

CHAMBER ANGLES
MEASURED CLOCKWISE
FROM INJECTOR
REFERENCE MARK AS
VIEWED LOOKING
UPSTREAM

INCREASE DUE TO THE
DELETION OF ELEMENT NO. 9

AXIAL LOCATION, in.

RUN NO.	ANGULAR ORIENTATION OF AXIAL THERMOCOUPLE ARRAY, °	NO. OF ELEMENTS
□ 705	315	52
▽ 706	310	52
× 707	320	52
▽ 708	45	52
△ 720	200	52
○ 723	200	51 *

*(NO. 9 DELETED)

RMIR INJECTOR NO. 5 WITH
M521 CHAMBER

CORPORAL PROPELLANTS

$r = 2.80^{+0.08}_{-0.04}$

$F \cong 20,000$ lb

$L^* = 40$ in.

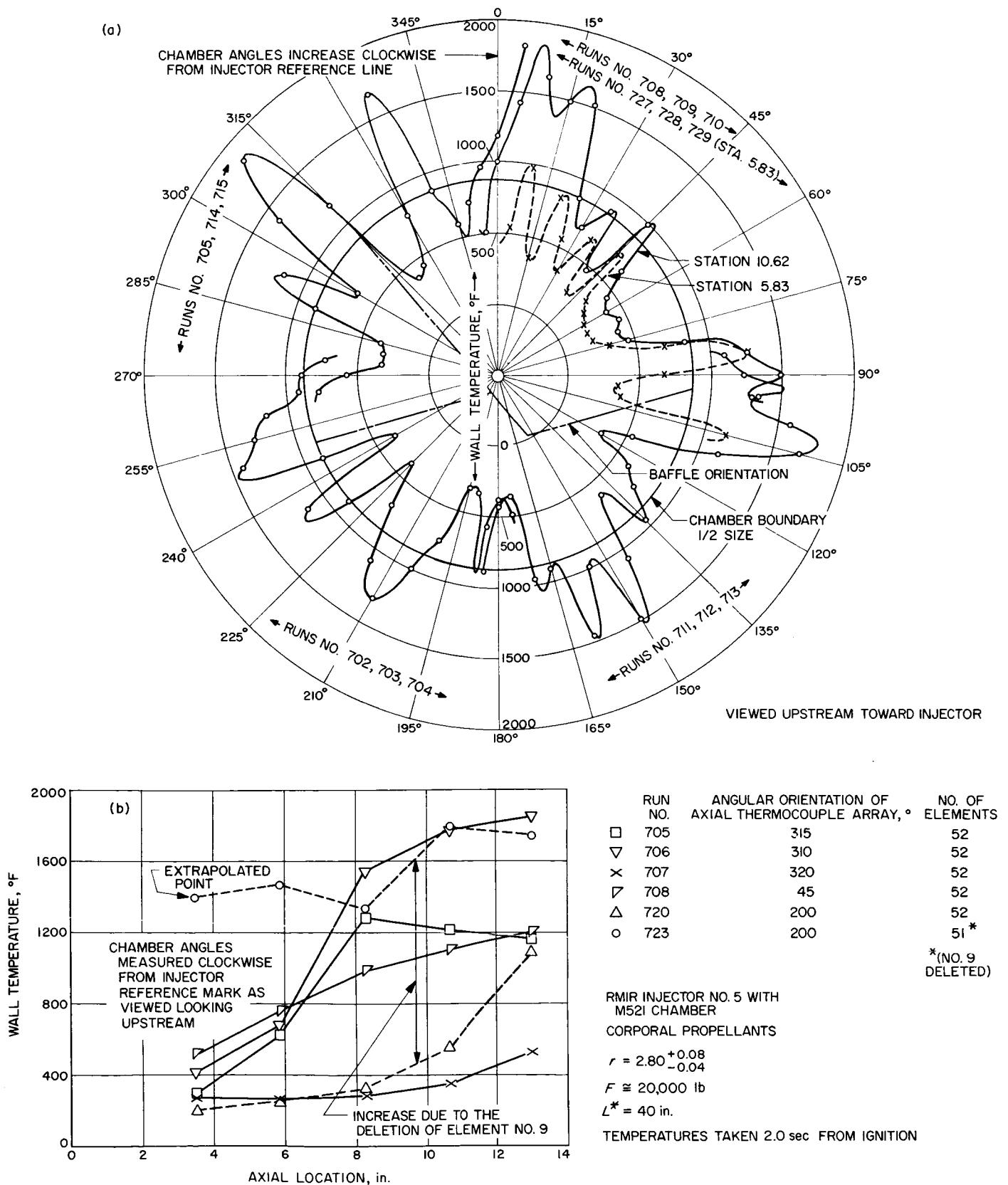TEMPERATURES TAKEN 2.0 sec FROM IGNITION

Fig. 7. Temperature distributions in an uncooled Corporal chamber with RMIR Injector No. 5 at constant mixture ratio

conditions and heat flux rates which apparently was not completely attenuated even by the flow processes occurring within the nozzle.

It is of interest to examine in more detail a flow phenomenon that was probably produced in the chamber as a result of this particular injector configuration. Observe the arrangement of injector elements shown in Fig. 4. Each of the 52 patterns depicts the distribution of mass from an injection element as it is seen on the model plane. The boundary of each element pattern represents the cross-sectional area associated with the mass of the element at the model plane. Consider for the moment the *non-reactive aspects* of the mass impingement process on the wall. If, for instance, a solid surface were brought adjacent to the outer boundary of a typical element, then, at the model plane distance, one would expect most of the liquid to just miss the surface. If, however, the surface were to be moved inside the element boundary, appreciable mass would strike the wall prior to reaching the model plane distance and form a film running down the wall past the model plane at that point. This flow would then be supplemented by the mass flux impinging directly on the wall at that point. Since the size of the mass distribution pattern enlarges as its distance from the impingment point is increased, the mass from a given element that had a radially outward velocity, but which had not yet arrived at the boundary at a specified distance, would ultimately strike the wall at a point further downstream. It is seen from the arrangement shown in Fig. 4 that several of the elements are already supplying mass to the boundary of the chamber at the model plane distance, since their mass distribution patterns have already intersected the wall. Further down the chamber, dispersion of the flow from the element increases, and more of the elements adjacent to the boundary would contribute mass to the chamber wall. Because the majority of the fluid particle trajectories lie in planes that are skew to the chamber wall, the flow direction of the liquid that impinges on the wall will, in general, have circumferential as well as axial velocity components. It is likely, therefore, that the flow running down the chamber wall will not follow a simple axial path, but will instead travel in the direction of the net momentum vector of the flow striking the wall.

These observations are further substantiated by the inferences that can be drawn from the data shown in Fig. 8, which compares one quadrant of the same mass flux analogue presented in Fig. 4 with the temperature distribution on the chamber boundary at station 5.83. Obviously this comparison is not quantitative, but the near one-to-one correspondence between high mass flux on the wall and gross temperature variations is undeniable. A comparison of these data with the temperature distributions shown in Fig. 7 also reveals a marked similarity in the temperature distributions at the two axial stations, if some allowance is made for the smearing effect one might expect in the boundary flow as it moves downstream.

Of course, combustion processes that are going on simultaneously in the chamber will further modify the nonreactive flow descriptions given above so that it would be completely fortuitous to find an obvious correlation between the circumferential temperature distribution at the 10.62-in. axial station with the mass distribution at the model plane. Yet it seems very clear that the gross variations in the observed temperature data must stem from the mass distributions initiated by the injection scheme and therefore must, at least in part, be relatable to them.

B. The Influence of Mixture Ratio Variations

Fig. 9 shows the data obtained 2.0 sec after the start of the run at typical chamber locations as the mixture ratio r was varied from 1.93 to 3.17. It is seen that, in most instances, substantial changes in the measured wall temperatures occurred as a function of the mixture ratio and that no unique relationship is apparent. In fact, some locations experienced increases in temperature while others became cooler for the same change in r. For comparative purposes the theoretical equilibrium gas temperature for this propellant combination, corrected by the factor $(c^*_{exp}/c^*_{th})^2$, is also shown. It is seen that the gross wall temperature data cannot be directly related to changes occurring in the gas temperature, nor is there any substantiating evidence to indicate a gross change in the gas-side film heat-transfer coefficient. Hence, it would appear likely that the differences noted in the data arise from changes in the local flow conditions on the chamber walls.

Non-reactive spray studies have shown that the distribution of mass within a spray formed by a doublet injection configuration is extremely sensitive to changes in the momentum ratio (or mixture ratio) of the two jets (Ref. 10). It is certain that the mass flux impinging on the boundary from the elements adjacent to the wall would be expected to reflect these changes. Hence, if the hypothesis be true that the mass flux reaching the boundary tends to play a dominant role in controlling
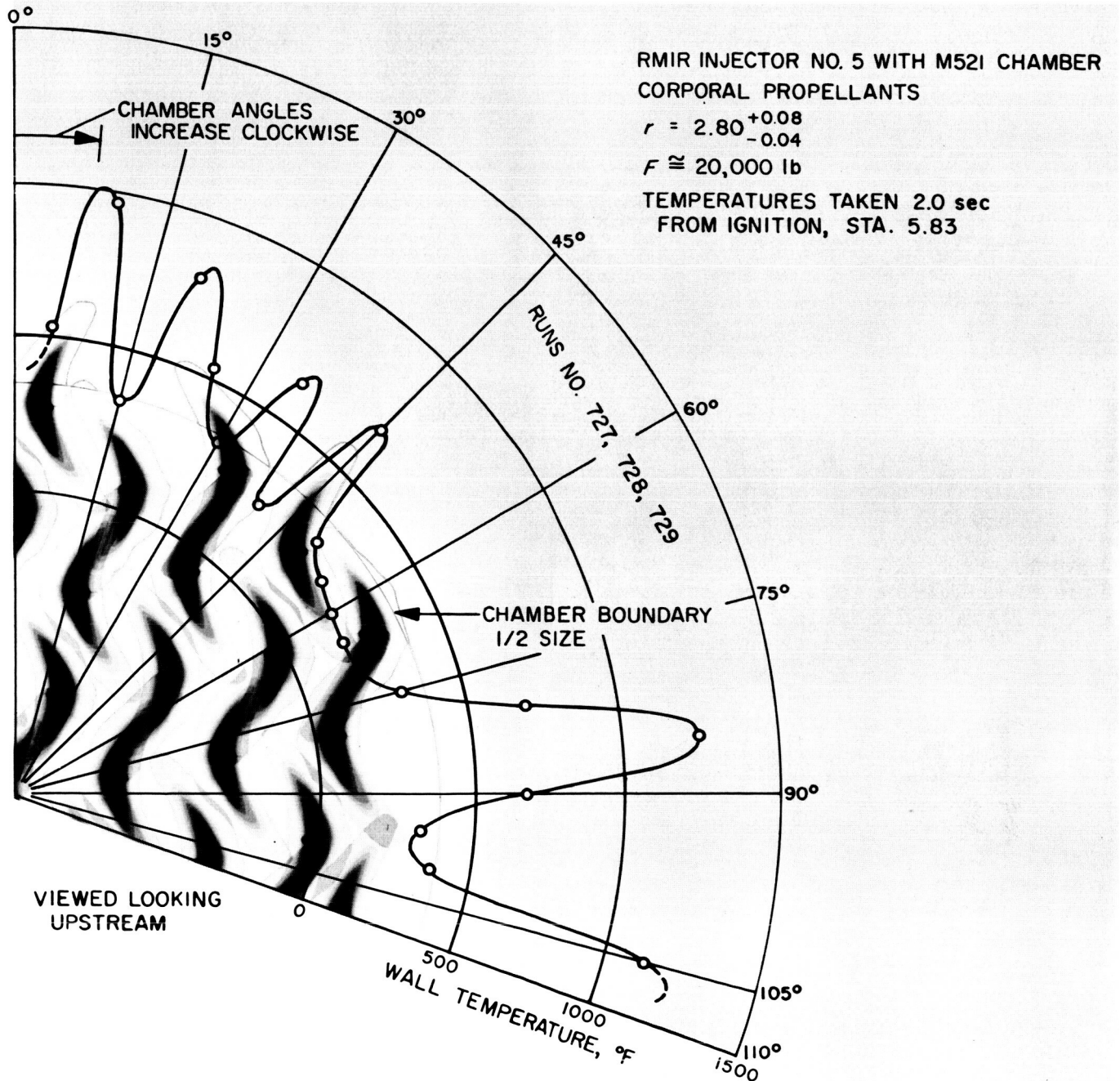
Fig. 8. Comparing axial mass flux distribution at Station 2.75 with temperature distribution at Station 5.83

the heat flux on the combustion chamber wall, then the observed heat flux variations would be expected. While such evidence is circumstantial at best, it does tend to lend credence to the hypothesis. It is interesting to note that the very large circumferential gradients are reflected here also. For example, a change in r from 2.58 to 2.62 resulted in a temperature change of 500°F for the thermocouple located at station 12.00.

Fig. 9. The effect of mixture ratio variation on local temperature in an uncooled Corporal chamber with RMIR Injector No. 5

IV. RELATING GROSS CHANGES TO LOCAL HEAT TRANSFER
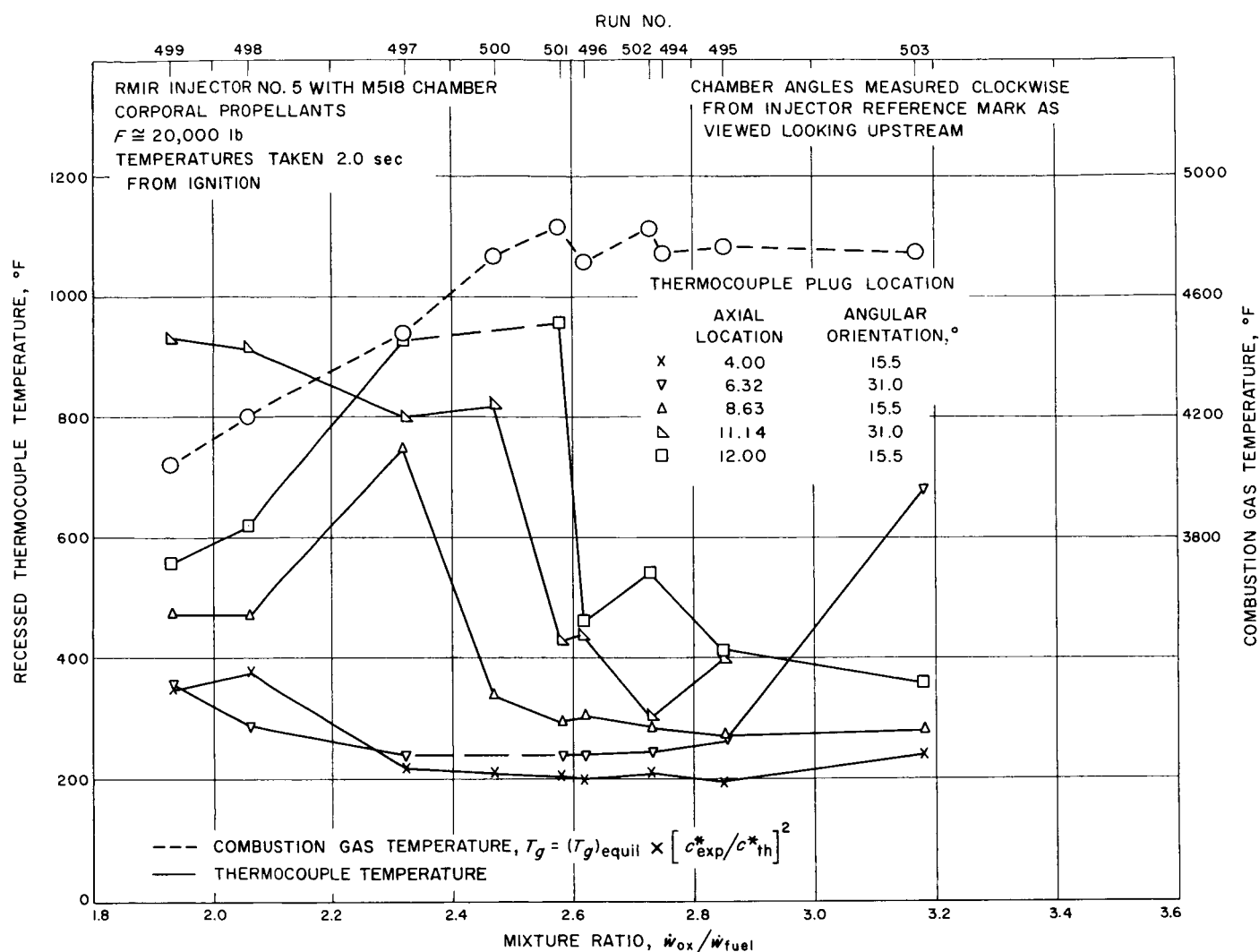
A. Calculation of the Mass Distribution on the Chamber Wall

In view of the fact that these initial experiments had indicated an intimate relationship between the mass flux produced by injector elements near the boundary and the heat flux at the wall, it seems appropriate to attempt to correlate these two parameters even though, in the former case, the data to be used were obtained with non-reactive fluids. This approach necessarily requires the very brash assumption that the effects of combustion upon the mass distribution are negligible, but it seemed to be warranted as a first step, in view of the difficulties associated with the determination of the boundary flow conditions in an actual combustion chamber.

In order to determine the mass flux to the wall, the following assumptions were required, together with the non-reactive properties of the spray from a typical injector element and its geometrical orientation in the chamber:

1. The mass distributions obtained for an element injecting propellants are similar to those produced by an identical element geometry and corresponding steam momenta, but with non-reactive fluids.

2. Spray particles travel in rays from the impingement point, which is assumed to be the spray source.

3. There is no interaction between neighboring sprays.

4. The mass distribution normalized for an element flow rate of 1.0 lb/sec does not change with level of flow rate.

5. Modifying effects due to spray combustion are negligible.

6. The previous history of the fluid striking the wall at adjacent locations and running along the wall can be disregarded.

7. Variations in heat flux due to varying composition (i.e., local r) are not important.

It follows from assumption 2 stated above that, if the local mass flux is known at a specific point in the spray, the mass flux rate can be estimated at other positions along the radial line that originates at the impingement point and passes through the point in question. It can be shown (Ref. 14) that the flow rate at any location along such a line is given by $G_1 = G_0 \times (L_0/L_1)^2$, where G_0

and G_1 are the local mass flux rates on the given line corresponding to the distances L_0 and L_1 respectively, as measured from the impingement point. Thus, if the flow rate distribution of a particular element is known on a spherical surface of a given radius, for instance, then the mass flux distribution on any other surface may be found. The local mass flow rates for a given element were experimentally determined by a spray-sampling apparatus that measured the mass flux seen on a spherical surface having a 6-in. radius, and so such data were readily adaptable to this computational procedure. Assumption 4 was required, however, since the sampled flow rate was not exactly equal to the flow rate per element in the injector.

By taking into account the physical location of a given element in the chamber, and by using the appropriate geometrical factors to relate the orientation of the mass distribution pattern to the wall of the chamber, it is possible to determine the true angle between the vector representing the direction travelled by a particle from its source and the normal to the tangent plane at the point of intersection with the chamber wall. If this angle is denoted as ξ, then it is possible to determine the mass flux normal to the wall by multiplying the equation above by $\cos \xi$, so that the component of the mass flux arriving at the wall is given by $G_w = G_0 \times (L_0/L_w)^2 \times \cos \xi$. Thus, repeated application of this equation yields the distribution of the normal component of the mass flux arriving at the wall. Moreover, by suitable summation procedures, the cumulative local mass flux that reaches the chamber wall as a result of the effect of all the injector elements acting together can thereby be established. The relative complexity of the intermediate mathematical steps that are involved, coupled with the vast number of calculations needed, required the use of an IBM 7094 digital computer to carry out the necessary computations. The results of these calculations are shown in Fig. 10a, which illustrates the local flux distribution on the chamber wall over a 90-deg sector of the boundary with all elements in place. Each contour represents a line of constant flow rate impinging on the wall per unit wall area for the values noted, and hence, in company with a series of constant mass-flux lines, portrays the mass flux distribution.

It is noted that, pursuant to assumption 6 stated above, the mass flux represented in Fig. 10 is that which would strike the wall at a given location, but does not include
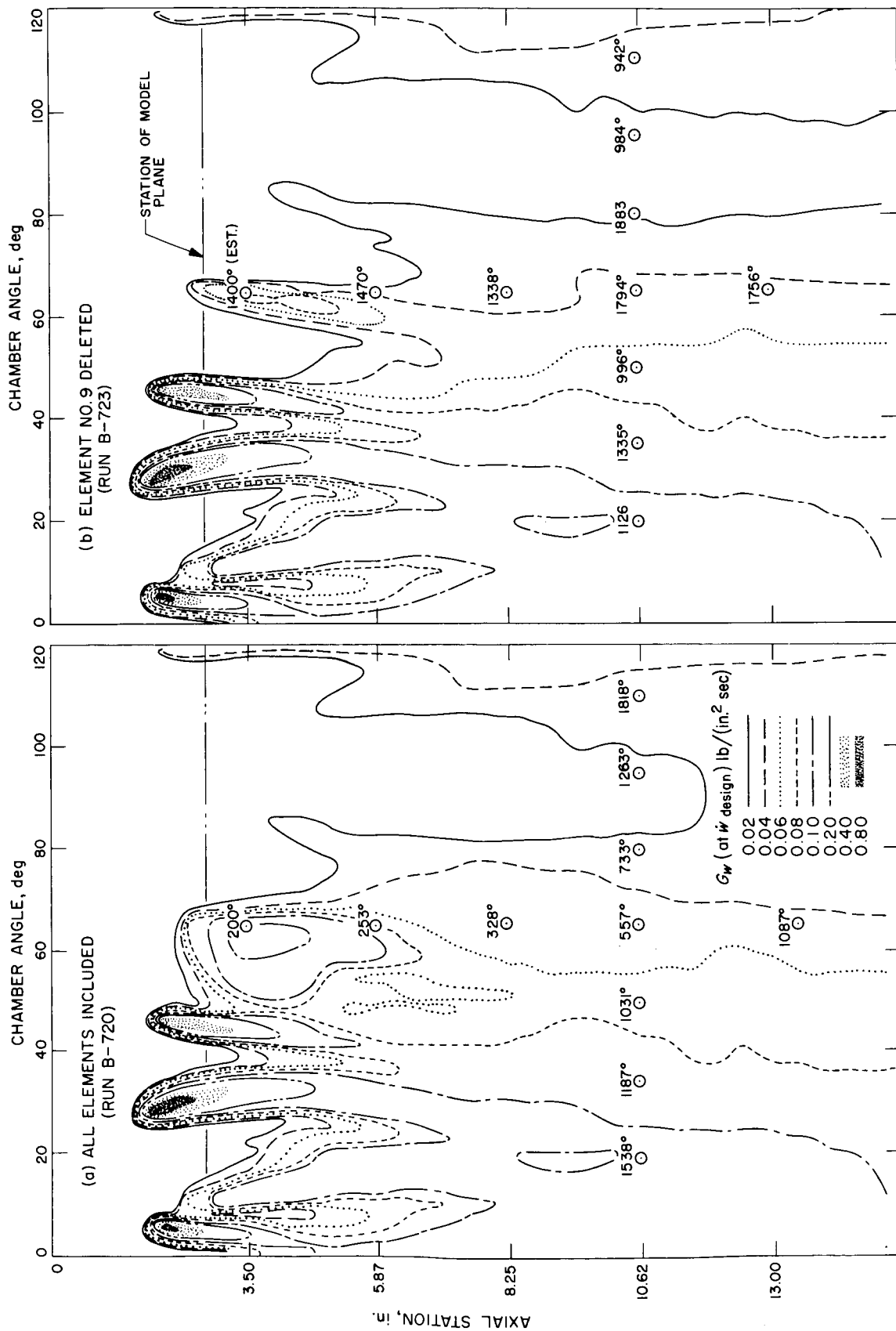
Fig. 10. Mass flux distribution on the wall of an uncooled Corporal chamber with RMIR Injector No. 5.(a) All elements (b) Element No. 9 deleted

the mass that may also be present at that location because of liquid flowing on the wall due to fluid impingement in adjacent regions. It is apparent that a grossly simplified model has been set forth to represent what, in actuality, is an exceedingly complex set of fluid dynamic and combustion processes.

B. Deletion of an Element

In an effort to further substantiate the premise that the nonuniform heat flux observed in the chamber could be related, at least in part, to the localized boundary conditions resulting from the injection scheme used in this engine configuration, it was decided to evaluate the changes in heat flux associated with the deletion of a single injection element located near the wall. It was expected that such a deletion would produce an immediate and obvious change in the mass arriving at the wall in that vicinity and that this, in turn, would markedly change the wall temperature distribution in the chamber in that area. The selected element is shown in Fig. 4 and is identified as element No. 9. Since each orifice was individually connected to its propellant manifold by a flexible hose, it was a relatively simple task to disconnect the two orifices involved. This particular element was chosen for deletion because it appeared likely that the amount of propellant reaching the wall in its vicinity would be radically changed as a result of its removal, and because severe temperature gradients had been observed in the same region. No other changes were made in the operating conditions of the engine, the mixture ratio remaining at 2.80, and the flow rate per element being held constant so that the total injected propellant was, therefore, 51/52 of its original level. Thus the boundary flow conditions as induced by the injection scheme would be unchanged except in the region of the deleted element.

The mass flux to the wall that is obtained by deleting this one element was calculated as before and is presented in Fig. 10b. A comparison of this distribution with the one shown in Fig. 10a for all elements in place reveals a substantial change in the pattern in the vicinity of 55 deg, particularly in the upstream portion of the chamber. Superimposed upon these distributions are the temperatures (measured 2.0 sec from ignition) that are associated with the indicated locations on the wall and hence the corresponding mass flux patterns. It is observed that the largest differences in the two sets of temperature data occurred in the region of the largest changes in the mass distributions; but as yet, a quantita-

tive correlation of these two parameters has not been achieved. Thus, even though such evidence is not conclusive *per se,* it does again suggest that an understanding of the heat transfer processes in a combustion chamber cannot be complete without a careful investigation of the local boundary phenomena.

It should be noted that it is our intention to present in a later publication a more detailed description of the analytical techniques outlined above, as well as some additional information on mass flux distributions produced by various other injection schemes.

C. Calculation of Heat Transfer Coefficient

The determination of local heat flux in the combustion chamber by means of transient temperature measurements permits additional information to be inferred regarding other boundary wall conditions. Since a lack of adequate information regarding local flow phenomena precludes a detailed analysis from being made, a simple convective heat transfer model is conventionally chosen to describe the mass- and heat-transport processes occurring in the engine. The relationship is usually written as $q = h (T_g - T_w)$, where q is the heat flux rate; h, the over-all gas-side heat-transfer coefficient; T_g, the combustion gas temperature; and T_w, the wall temperature on the gas side of the wall.

If it is assumed that the steady-state values of chamber pressure, characteristic velocity, and thrust that are achieved early in the run are indicative of steady combustion conditions, then it is reasonable to expect that flow conditions at the boundary of the combustion chamber are also established shortly after the start of the run. Of course, when uncooled hardware is used, boundary wall temperatures continuously rise during the run; these temperatures, in turn, will affect boundary flow conditions to a degree throughout the run period. However, over a short time interval, the boundary layer flow can be considered to be quasi-steady. The gas-side film heat-transfer coefficient h is a wall-temperature-dependent parameter but, if it is assumed that over a short time period the wall temperature does not substantially change (or that h is relatively insensitive to small temperature changes), then, over the time interval in question, h can be considered to be constant. By using the experimentally measured values of q and T_w at the beginning and end of the time period, values of h and T_g may be determined if it is further assumed that T_g is invariant over this time interval. Thus if subscripts 1 and

2 denote conditions at two temporally adjacent points in the run, then the following equations can be written

$$q_1 = h_1 \left(T_{g_1} - T_{w_1} \right) \tag{2}$$

and

$$q_2 = h_2 \left(T_{g_2} - T_{w_2} \right). \tag{3}$$

If it is assumed that $h_1 = h_2 = h$ and $T_{g_1} = T_{g_2} = T_g$, it follows from Eq. (2) and (3) that

$$h = \frac{q_2 - q_1}{T_{w_1} - T_{w_2}} \tag{4}$$

and

$$T_g = \frac{q_2 \, T_{w_1} - q_1 \, T_{w_2}}{q_2 - q_1}. \tag{5}$$

Application of Eqs. 4 and 5 to the experimental data obtained during a typical series of runs at a mixture ratio of 2.80 produced notably different values of T_g and h at various circumferential locations in the chamber at the 10.62-in. station. These data are summarized in Table 1. It should be noted that the results shown were computed from data obtained with the *same* thermocouple plug. The several different locations evaluated were reached by rotating the chamber relative to the injector the appropriate number of degrees. In order to smooth the experimental data, curves were fitted to both

the heat flux–time distributions and the temperature–time distributions, and the values chosen for the computations were read from the curves. It should be noted that the time period chosen for these calculations was 0.2 sec and that additional variations in the calculated parameters are introduced if this period is varied.

In general, the values of T_g determined in this manner were considerably *lower* than the magnitude of this parameter predicted from equilibrium combustion considerations (cf. Fig. 9). In two instances, however, the temperatures were much higher than those expected. While one might argue that such differences are a result of inappropriate simplifying assumptions regarding the constant value of h, it is more probable that they reflect either the inadequacy of the gas-side convective heat-transfer model or the result of nonequilibrium combustion products reaching the walls. The main point to be recognized is that the simple convective heat transfer model used in the calculations above is woefully inadequate to cope with flow phenomena such as a liquid film on the wall. Until a method becomes available to ascertain and account for local combustion conditions as well as boundary flow effects, the accurate prediction of heat transfer rates, or for that matter any other local property, in the combustion chamber of a rocket engine will not be possible.

Table 1. Effective free-stream gas temperatures and convective heat transfer coefficients as determined from experimental heat flux and temperature data

Run no.	Chamber orientation deg	Data computed at 1.5 sec from ignition		Data computed at 2.0 sec from ignition	
		h Btu/(in.^{2} sec °F)	T_g °F	h Btu/(in.^{2} sec °F)	T_g °F
702	195	0.0018	690	0.0043	440
703	200	0.0039	1,160	0.0083	970
704	190	0.0100	400	0.0066	490
705	285	0.0020	690	0.0022	640
709	20	0.0006	9,540	0.0005	8,340
711	100	0.0011	4,790	0.0008	10,460
714	280	0.0250	320	0.0100	365

All data were measured with the same thermocouple plug (195-10.62) at station 10.62 in chamber M521.

Mixture ratio $r = 2.80 \, {}^{+0.08}_{-0.04}$ for runs shown.

Chamber pressure $p_c = 309.5 \, {}^{+3.7}_{-3.5}$ psia for runs shown.

Characteristic velocity $c^* = 4894 \, {}^{+12}_{-18}$ ft/sec for runs shown.

Faired temperature and heat flux data were used.

Chamber angles were measured clockwise from injection reference mark as viewed looking upstream from nozzle.

V. HEAT TRANSFER DURING RESONANT COMBUSTION

As mentioned earlier, resonant combustion was encountered with this engine configuration during the initial stage of the experimental program (i.e., prior to the use of baffles). During the period when this problem was being evaluated, a limited amount of heat transfer data was obtained during unstable engine operation. It is intended that these combustion characteristics be described in greater detail in a later publication, but in view of the rather extreme nature of the disturbances that have been observed it is perhaps pertinent to review them here. In particular, attention will be paid to those aspects that tend to influence heat transfer rates.

It should first be recognized that when the engine is operating in a nonresonant mode the small pressure variations associated with the chemical reaction mechanisms (1 to 2 psi rms) are considered to occur in a random manner. Although the combustion may be smooth or even rough (i.e., with large, but necessarily random, chamber pressure fluctuations), there is no time dependence or periodicity in the pressure perturbations. As a

consequence of the relatively gradual release of energy in the chamber under these conditions, a more or less tolerable heat transfer rate usually results. On the other hand, when resonant or unstable combustion takes place, the entire character of the energy release process and, therefore, the heat transfer mechanism, is radically changed. No longer are the pressure variations completely disordered; instead, periodic and often quite severe pressure oscillations are observed. It is currently believed that these periodic pressure perturbations are initiated as a result of the sudden release of energy behind small pressure disturbances traveling through regions of partially unreacted propellants in the chamber. The rapid combustion behind the disturbance raises the pressure in that region and, hence, tends to reinforce the pressure wave until it grows into what, in this engine, seems to be a moving detonation wave. These waves apparently couple with the engine geometry and are manifest in what appear to be circumferentially traveling waves. The passage of such a wave through the unburned and/or reacting propellants in the chamber ap-
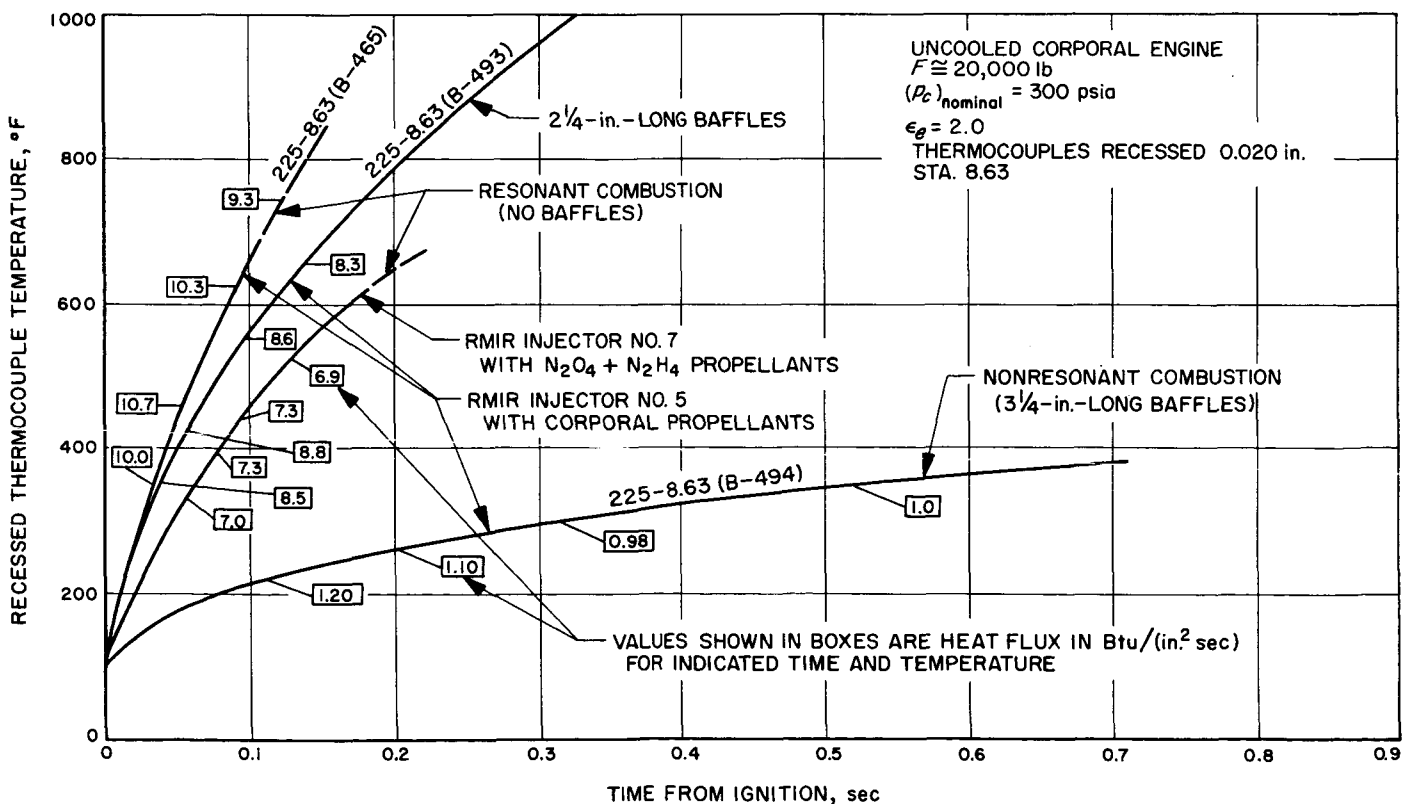

Fig. 11. Variations in heat transfer due to resonant combustion for a particular chamber location

parently enhances the reaction rates of the constituents, so that the resulting reaction completely consumes the propellants behind the wave in an extremely rapid fashion. The pressure disturbances encountered in this engine during unstable operation were characterized by pressure waves having amplitudes of 1000 psia or more, and they appeared to propagate around the combustion chamber near the injector face at a speed of approximately 1800 rps to give a velocity of the intersection of the disturbance with the boundary of about 7000 ft/sec. It is certain that the interaction of these pressure fronts with the chamber boundary will modify the boundary layer conditions in a manner that would adversely affect the thermal barrier usually associated with such boundary layer flow. These changes, together with the high reaction rates behind the pressure wave, probably account for the unusually severe heat transfer rates that were observed.

The onset of resonant combustion is identified by an abrupt change in the rate of change of temperature with time throughout the chamber. This can be seen from the data given in Fig. 11, which shows the temperature–time history at a given chamber location for several

significantly different resonant environments and compares them with a "typical" nonresonant transient. In each case, the heat flux associated with several particular times during the transient are indicated. It is particularly interesting to note with RMIR Injector No. 5 that the addition of a subcritical-length baffle reduced the amplitude of the disturbance from about 1500 psi to approximately 200 psi, while reducing the heat flux by only 25%. Further, the extension of the length of the baffle by an additional inch reduced the pressure disturbances to a negligible value and produced a large decrease in heat flux. The over-all effect is to produce a decrease of almost an order of magnitude in heat flux as the transition from resonant to nonresonant combustion takes place.

Figure 12 is an attempt to illustrate the variations in the axial distributions that occur for those same variations in operating conditions. It is clear that the scatter in the data precludes any truly definitive conclusions. However, the same general relationships shown in Fig. 11 prevail at any given axial station and, in addition, it is seen that there is a progressive change in the characteristics of the axial distribution as the severity of the
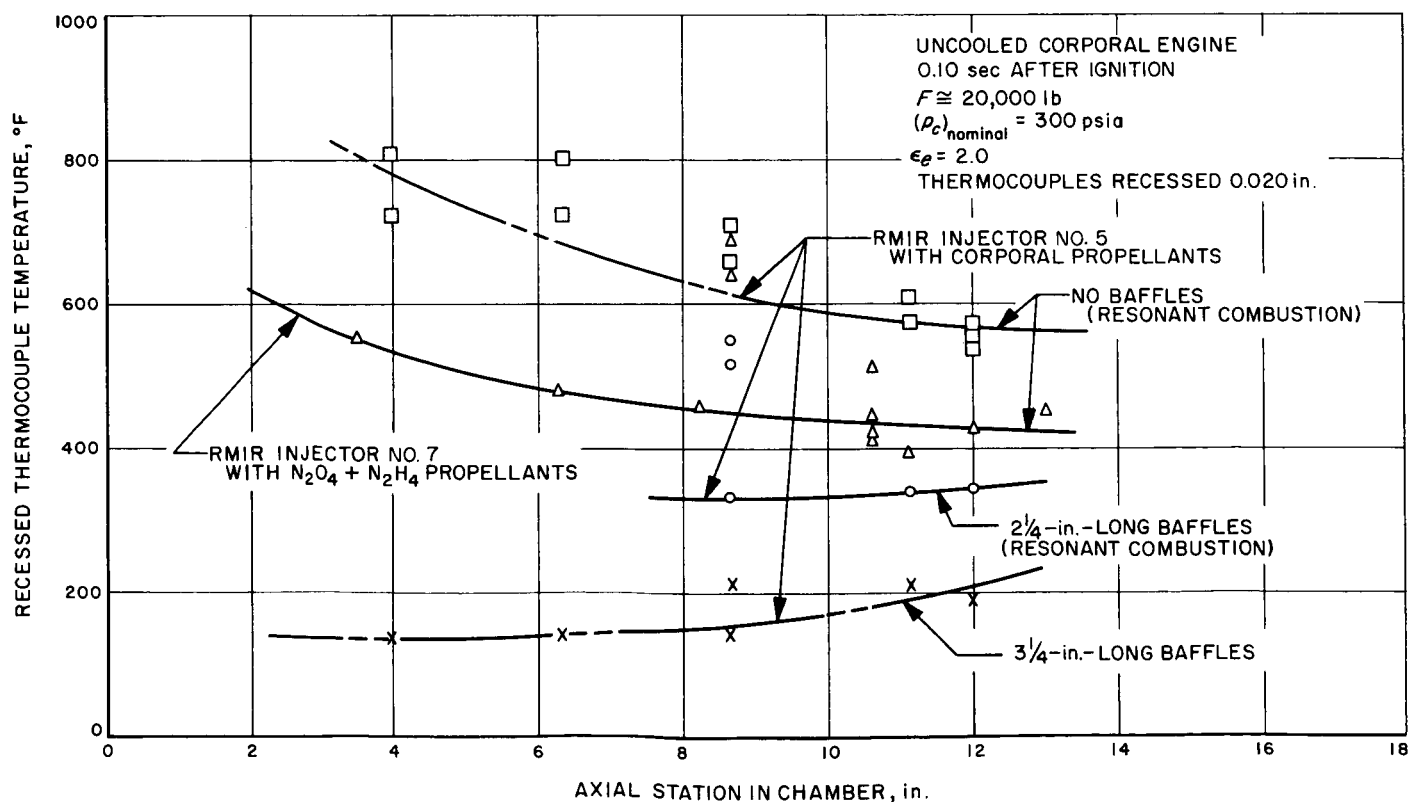

Fig. 12. Variations in transient temperature distributions due to resonant combustion

disturbance increases. In particular, the heat flux tends toward a maximum at the nozzle inlet with stable combustion, while the maximum occurs near the injector end of the chamber during resonant combustion. Moreover, the magnitude of the heat flux at the nozzle inlet tends toward a common value, indicating the establishment of similar boundary conditions, presumably because similar, near-equilibrium velocities are attained in both combustion modes. It should further be noted that local variations in the mass distribution, either in the chamber or on the chamber walls, tend to be overwhelmed by

these high-amplitude disturbances and, therefore, have little or no effect upon heat transfer data obtained during unstable combustion.

For reference purposes only, these figures also include comparable heat transfer characteristics obtained with a somewhat different injection scheme (i.e., RMIR No. 7), using the propellant combination N_2O_4 and N_2H_4. It is noted that the heat flux for this system during resonant combustion is somewhat lower than that for the RMIR Injector No. 5–Corporal propellant system.

VI. SUMMARY OF RESULTS AND CONCLUSIONS

1. Local heat flux and/or temperature measurements obtained in a rocket engine chamber are, in general, not representative of the "average" value of these parameters. Relatively complete sampling must be made to determine the maximum values and/or assure that an assumed uniformity of conditions has, in fact, been achieved.

2. Experiments involving the deletion of an injector element, along with an analytical procedure used to compute the mass flux on the chamber boundary, suggested that a close relationship exists between the heat flux at the wall and the mass flux produced by injector elements. This was further substantiated by the reasonably good agreement seen between the temperature distribution and the mass flux analogue model.

3. Significant variations in both the axial and circumferential distributions of temperature were observed.

Appreciable changes were noted in these distributions as a function of mass distribution variations resulting from changes in mixture ratio.

4. Computations based on a simple, convective heat transfer model showed the inadequacy of such a method, and pointed up the necessity of taking into account local boundary flow effects.

5. Heat flux measurements made during resonant combustion indicated an almost order-of-magnitude increase over similar measurements made during stable engine operation.

6. The understanding and ultimate prediction of heat transfer in a rocket engine combustion chamber will be possible only after the pertinent boundary flow phenomena are understood and can be predicted.

NOMENCLATURE

Symbols

A area, in.^{2}

c^* characteristic velocity, ft/sec

C_d discharge coefficient

C_f thrust coefficient

c_p specific heat capacity at constant pressure, Btu/(lb °F)

d diameter, in.

F thrust, lb

G mass flux per unit area, lb/(in.^{2}sec)

h gas-side heat-transfer film coefficient, Btu/(in.^{2} sec °F)

I_s specific impulse, sec

k thermal conductivity, Btu/(in.^{2} sec °F/in.)

L length, in.

L^* characteristic length of combustion chamber, in.

N number of elements

p pressure, lb/in.^{2}

q heat flux, Btu/(in.^{2} sec)

R radius, in.

r mixture ratio

T temperature, °F

t time, sec

$\dot{w}$ weight flow rate, lb/sec

β complement of true angle between resultant momentum line of injector element and plane normal to chamber axis, deg

γ specific heat ratio

ϵ_c nozzle–contraction area ratio

ϵ_e nozzle–expansion area ratio

λ nozzle divergence loss factor

ξ angle between particle director vector and normal to wall at point of intersection, deg

ρ density, lb mass/ft^3

Subscripts

B boundary

c chamber

e expansion

exp   experimental

g conditions in gaseous combustion products

ox   oxidizer

t throat

th   theoretical

w condition at wall

REFERENCES

1. Bartz, D. R., "An Approximate Solution of Compressible Turbulent Boundary-Layer Development and Convective Heat Transfer in Convergent-Divergent Nozzles," *Transactions of the ASME,* Vol. 77 (No. 8), pp. 1235–1245, November 1955.

2. Bartz, D. R., "A Simple Equation for Rapid Estimation of Rocket Nozzle Convective Heat Transfer Coefficients," *Jet Propulsion,* Vol. 27 (No. 1), pp. 49–51, January 1957.

3. Rose, R. K., "Experimental Determination of the Heat Flux Distribution in a Rocket Nozzle," M.S. Thesis, Purdue University, January 1958.

REFERENCES (Cont'd)

4. Neu, R. F., Comparison of Localized Heat Transfer Rates in a Liquid-Oxygen–Heptane Rocket Engine Employing Several Injection Methods and Oxidant-Fuel Ratios, NASA TN D-286, June 1960.

5. Bartz, D. R., "Turbulent Boundary-Layer Heat Transfer from Rapidly Accelerating Flow of Rocket Combustion Gases and of Heated Air," *Advances in Heat Transfer*, Vol. II, ed. by T. F. Irvine and J. Hartnett, Academic Press Inc., New York (To be published).

6. Welsh, W. E., Jr., and Witte, A. B., "A Comparison of Analytical and Experimental Local Heat Fluxes in Liquid-Propellant Rocket Thrust Chambers," *Journal of Heat Transfer*, Vol. 8, Sec. C, No. 1, pp. 19–28, February 1962.

7. Witte, A. B., and Harper, E. Y., "Experimental Investigation and Empirical Correlation of Local Heat-Transfer Rates in Rocket-Engine Thrust Chambers," *AIAA Journal*, Vol. 1, No. 2, pp. 443–451, February 1963.

8. Rupe, J. H., A Correlation Between the Dynamic Properties of a Pair of Impinging Streams and the Uniformity of Mixture-Ratio Distribution in the Resulting Spray, Progress Report No. 20-209, Jet Propulsion Laboratory, Pasadena, California, March 28, 1956.

9. Rupe, J. H., On the Dynamic Characteristics of Free-Liquid Jets and a Partial Correlation with Orifice Geometry, Technical Report No. 32-207, Jet Propulsion Laboratory, Pasadena, California, January 15, 1962.

10. Rupe, J. H., The Liquid-Phase Mixing of a Pair of Impinging Streams, Progress Report No. 20-195, Jet Propulsion Laboratory, Pasadena, California, August 6, 1953.

11. Rupe, J. H., An Experimental Correlation of the Non-reactive Properties of Injection Schemes and Combustion Effects in a Liquid-Propellant Rocket Engine: Part I. The Application of Non-reactive Spray Properties to Rocket Motor Injector Design, Jet Propulsion Laboratory, Pasadena, California (To be published).

12. Rupe, J. H., Jaivin, G. I., and Clayton, R. M., An Experimental Correlation of the Non-reactive Properties of Injection Schemes and Combustion Effects in a Liquid-Propellant Rocket Engine: Part III. On the Relationship Between Gross Performance Level and Injection Schemes, Jet Propulsion Laboratory, Pasadena, California (To be published).

13. Powell, W. B., Howell, G. W., and Irving, J. P., A Method for the Determination of Local Transient Heat Flux in Uncooled Rocket Motors, Technical Report No. 32-257, Jet Propulsion Laboratory, Pasadena, California, July 1, 1962.

14. Jaivin, G. I., Clayton, R. M., and Rupe, J. H., An Experimental Correlation of the Non-reactive Properties of Injection Schemes and Combustion Effects in a Liquid-Propellant Rocket Engine: Part IV. Relating the Injection Pattern to Heat Transfer to the Chamber Wall, Jet Propulsion Laboratory, Pasadena, California (To be published).